HHS Public Access

Author manuscript

Bone. Author manuscript; available in PMC 2018 October 01.

Published in final edited form as:

Bone. 2017 October ; 103: 116–124. doi:10.1016/j.bone.2017.06.015.

Non-Destructive NIR Spectral Imaging Assessment of Bone Water: Comparison to MRI Measurements

Chamith S. Rajapakse[1], **Mugdha Padalkar**[2], **Heejin Yang**[2], **Mikayel Ispiryan**[1], and **Nancy Pleshko**[2,*]

[1]Departments of Radiology and Orthopaedic Surgery, University of Pennsylvania, Philadelphia, PA USA

[2]Department of Bioengineering, Temple University, 1947 N. 12th St, Philadelphia, PA USA

Abstract

Bone fracture risk increases with age, disease states, and with use of certain therapeutics, such as acid-suppressive drugs, steroids and high-dose bisphosphonates. Historically, investigations into factors that underlie bone fracture risk have focused on evaluation of bone mineral density (BMD). However, numerous studies have pointed to factors other than BMD that contribute to fragility, including changes in bone collagen and water. The goal of this study is to investigate the feasibility of using near infrared spectral imaging (NIRSI) to determine the spatial distribution and relative amount of water and organic components in whole cross-sections of bone, and to compare those results to those obtained using magnetic resonance imaging (MRI) methods. Cadaver human whole-section tibiae samples harvested from 18 donors of ages 27–97 years underwent NIRSI and ultrashort echo time (UTE) MRI. As NIRSI data is comprised of broad absorbances, second derivative processing was evaluated as a means to narrow peaks and obtain compositional information. The (inverted) second derivative peak heights of the NIRSI absorbances correlated significantly with the mean peak integration of the water, collagen and fat NIR absorbances, respectively, indicating that either processing method could be used for compositional assessment. The 5797 cm^{-1} absorbance was validated as arising from the fat present in bone marrow, as it completely disappeared after ultrasonication. The MRI UTE-determined bound water content in tibial cortical bone samples ranged from 62 to 91%. The NIRSI water peaks at 5152 cm^{-1} and at 7008 cm^{-1} correlated significantly with the UTE data, with $r = 0.735$, $p = 0.016$, and $r = 0.71$, $p =$. 0096, respectively. There was also a strong correlation between the intensity of the NIRSI water peak at 7008 cm^{-1} and the intensity of the collagen peak at 4608 cm^{-1} ($r = 0.69$, $p = 0.004$). Since NIRSI requires minimal to no sample preparation, this approach has great potential to become a gold standard modality for the investigation of changes in water content, distribution, and environment in pre-clinical studies of bone pathology and therapeutics.

Graphical Abstract

*Corresponding author: Department of Bioengineering, Temple University, 1947 N. 12th St., Philadelphia, PA 19122 USA., Tel.: +1 2152044280., npleshko@temple.edu.

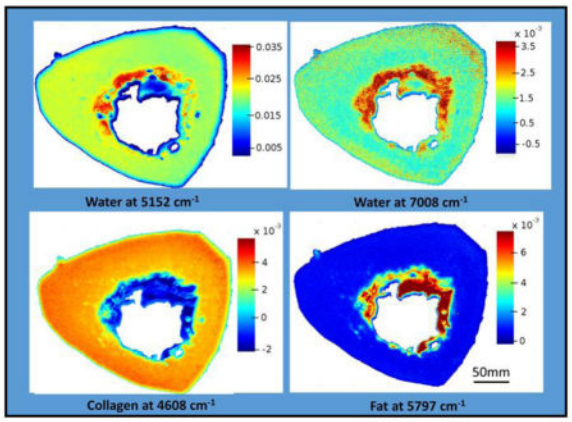

Keywords

Near infrared spectroscopy; Magnetic Resonance Imaging; UTE; Bone; Fracture; Water

1. Introduction

The risk of bone fracture is known to increase with age, disease states (including osteoporosis, osteogenesis imperfecta (OI), renal osteodystrophy, and diabetes) [1–6], and with use of certain therapeutics, such as acid-suppressive drugs [7], steroids [8] and high doses of bisphosphonates [9]. Historically, investigations into factors that underlie bone fracture risk have focused on evaluation of areal bone mineral density (aBMD) [1, 3]. Accordingly, current clinical practice utilizes assessment of aBMD by dual-energy X-ray absorptiometry (DXA) as the main modality for prediction of fracture risk. However, numerous studies have pointed to more complex factors at multiple scale lengths that contribute to bone fragility[10], including bone geometry and microarchitecture [11–13], collagen content and crosslinks [14–16], mineral crystallinity and heterogeneity [17], and, of increasing focus, water content [18–20]. In fact, studies have demonstrated age-related increases in fracture risk that occur without changes in bone mineralization [21, 22] and that may be attributable to alterations in bone water[23].

To fully understand the factors that contribute to bone fragility, appropriate methods of analysis of bone composition and structure are required. Although many aspects of bone composition and structure have been evaluated in depth, water content and environment (specifically, which components water is bound to) has not, due to the lack of tools. For evaluation of bone architecture at the micron level, micro computed tomography (CT) is widely utilized in animal studies [12, 13, 24], and high resolution peripheral quantitative computed tomography (pQCT) [1, 11, 25, 26] and MRI [4, 27, 28] are increasingly used for studies in human. For assessment of mineral properties in harvested tissues, Fourier transform infrared spectroscopic imaging (FT-IRIS, based on infrared radiation in the mid-infrared spectral region) has proved to be a powerful technique that can provide information on mineral composition at ~ 6 microns pixel resolution, including mineral phase, relative density, crystallinity, carbonate substitution, acid phosphate substitution, and heterogeneity [29–35]. Data from these studies have yielded insight into mineral compositional changes in

animal models of bone disease [30–32], and into changes in bone from patients treated with bisphosphonates [30, 35]. However, in the spectral regions of interest, there is limited depth of penetration, and thus these studies require thin histological sections of bone (3 to 5 microns thick) for analysis. This results in small volumes of dehydrated tissue as the basis for such studies, which precludes evaluation of the contribution of water. Raman spectroscopy has also been utilized to assess mineral composition, and has the advantage of a greater depth of penetration, and thus can be applied to intact bone [36, 37]. Mineral phase and crystallinity can be investigated with Raman spectroscopy at a spatial resolution of ~ 1 micron, however it offers limited signal to noise ratio. Therefore, to date, the use of this modality has been more limited than FT-IRIS studies [37, 38]. Both FT-IRIS and Raman have been applied to evaluate collagen quality in harvested bone tissues, with investigations focusing on both enzymatic crosslinks [37, 39] and non-enzymatic crosslinks in the form of advanced glycation end products [40, 41]. Even with the molecular-level information available from such spectroscopic studies, investigations into water interactions in intact bone have been limited [42], and have not included imaging investigations of tissues. Gravimetric analysis is still the standard method for assessment of water in tissue, a destructive technique that does not permit imaging of water distribution.

Ultra-short echotime magnetic resonance imaging (UTE-MRI) provides increased access to short T2-species, with applications to bone in a clinical environment increasing substantially in recent years. Use of UTE-MRI for non-invasive evaluation of water bound to collagen and water residing in pore spaces in bone is based on the well-founded notion that the transverse relaxation time of bound water is substantially shorter than that of free (pore) water [43–45]. Progress has been made on the validation of the use of UTE-MRI for evaluation of these two broad categories of bone water [44–49]. In these studies direct visualization of water compartments is not performed, since the micron or sub-micron pore sizes remain much smaller than the resolution capabilities of MRI. In one study, differences in overall bone water concentrations were found between pre- (18%) and post- (29%) menopausal volunteers, as well as in comparison to a volunteer with renal osteodystrophy (40%), without differences in bone density [23]. Recently, the feasibility of using UTE-MRI measured bound and free water for volumetric mapping of cortical bone porosity in human subjects have been demonstrated [45] Further, an in vivo UTE-MRI study in beagles showed changes in bone water content with raloxifene treatment, providing evidence that drug-induced changes in skeletal hydration can be noninvasively assessed using this technique [50]. Although these results are encouraging, there are several challenges for clinical translation. The percentage of free water in bone can be as low as 4% of the total water [51] so that evaluation of changes in this parameter with disease or treatment could require a very high degree of accuracy and precision. More importantly, these techniques cannot map bound and free water in cortical bone at spatial resolutions beyond imaging resolution, which is on the order of 0.5mm for whole bone cross section studies[45]. Recently, a custom built short wave Raman spectrometer was utilized to investigate water in bone at high spatial resolution, but such analyses would be challenging using standard Raman spectrometers [42, 52].

Near-infrared spectroscopy (NIRS) is the gold-standard technique for determination of water content and molecular composition in the food and pharmaceutical industries [53–57], in

large part due to its ability to evaluate intact samples, such as tablets and food mixes, with minimal or no sample preparation[53, 58–61]. It has also recently been utilized by our group to evaluate the water content in intact cartilage[62]. NIRS uses higher frequency (shorter wavelength) radiation than mid IR, permitting a much greater depth of penetration (millimeters to centimeters)[63]. The NIRS absorption bands arise from molecular vibrations, and are overtones and combinations of the mid-IR fundamental vibrations of C-H, C-O, O-H and N-H bonds. Therefore, they are widely used to monitor water, lipids, proteins and sugars, in spite of potentially much lower intensities. The absorbances from phosphate are very small in the NIR spectral region, and have not been widely used to monitor calcium phosphate compounds including bone apatite[64]. NIR spectral features are generally broad, with overlapping and low intensities, as they arise from combination and overtone absorbances of molecular vibrations[53]. Evaluation of NIR spectra is often coupled with multivariate chemometric analysis to obtain improved understanding of the spectral features[65]. In comparison, other vibrational spectroscopic techniques, such as, Raman and mid infrared (mid-IR), have narrower spectral features, and the absorbances arise from primary molecular vibrations that have been validated in multiple studies [66]. Raman and mid-infrared can also be applied in spectral imaging mode to obtain distributions of matrix components[34, 67]. One drawback of Raman spectroscopy is that there are challenges in data collection from samples that produce significant amounts of fluorescence, such as samples impurities[66, 68]. However, the two primary advantages of NIRS over the mid-infrared and Raman modalities are i)the penetration depth of the radiation, which permits evaluation of tissues through several millimeters or even centimeters[63], dependent on the specific wavelength range investigated, and ii) the ability to obtain information about water. When compared to UTE, NIR offers better spatial resolution (when coupled with an imaging spectrometer, ~6μm, and fiber optic probes, ~1mm). Although NIR can provide information about bound and free water as well as collagen content of the bone [62, 69], it has not been used to study mineral quality of the bone due to the fact that the phosphate absorbance is very low in the NIR region. For the mineral quality of the bone, Raman and mid IR are currently the preferred methods of analysis over NIR.

In the current study, we investigate the use of NIR spectral imaging (NIRSI) to define the spatial distribution and relative amount of water and organic components in whole cross-section of bone. NIR spectral imaging requires minimal to no sample preparation, and thus there is great potential for this modality to become the gold standard for the investigation of changes in water content, distribution and environment in pre-clinical studies of bone pathology and therapeutics. We also compared these data to water content as determined by MRI UTE studies.

2. Methods

2.1 Tissues

Cadaver human tibiae were harvested from 18 donors with no evidence of skeletal disease (5 male and 13 female), 12 of which were used for assessment of water (5 male and 7 female) of ages 27–97 years. (NDRI, Philadelphia, PA). Bones were stored frozen at −30° C, except when thawed for UTE-MRI data acquisition, and near infrared spectral data acquisition. For

UTE-MRI experiments, 36-mm whole cross-section specimens were cut from the diaphysis approximately 38% of the tibia length proximal to distal endplate using a reciprocating saw after thawing to room temperature. For IR experiments, 450 micron thick whole cross-section samples were utilized as described below. One sample thickness was utilized to eliminate the potential effects of thickness variation on spectral data.

2.2 UTE-MRI data acquisition and processing

The cortical bone specimens underwent three-dimensional UTE MRI in a 3-T whole-body clinical scanner (Siemens, Erlangen, Germany) using a surface coil (Insight MR imaging, Worcester, Mass). Imaging parameters were as follows: 12 msec repetition time, 12° flip angle, 50,000 half-projections distributed uniformly within a sphere, and 190 readout points per projection. Twenty-three UTE images were acquired at echo times 50, 64, 80, 100, 130, 160, 200, 250, 320, 400, 500, 640, 800, 1000, 1300, 1600, 2000, 2500, 3200, 4000, 5000, 6400, and 7790 μsec. UTE images were reconstructed onto a 320 × 320 × 320 matrix that corresponded to an isotropic 0.5 mm voxel size. Compact-appearing cortex that excluded the trabecularized transition zone was used for analysis as previously described[70]. This methodology was an operator-guided segmentation approach for carefully avoiding the trabecularized regions of the cortex. Bound and pore water fractions were assessed by bi-exponential fitting of the 23-echo UTE MR imaging data.

2.3 NIR Spectral Imaging (NIRSI) Sample Preparation

Samples were thawed, and to eliminate sample thickness as a variable in the analysis, whole cross-section specimens were cut to a uniform thickness of 450 μm from the regions of maximum cortical bone thickness (~38% distance proximal to distal endplate) with a diamond wafering saw (Buehler Isomet 1000, Lake Bluff, IL). The uniform thickness specimen was then stored in 12 mM phosphate buffered saline (PBS) solution (1x, pH 7.4, Invitrogen, Carlsbad, CA) at 4° C prior to data collection, typically for one or two days.

2.4 NIRSI data collection

NIR spectral images were collected from the 450 μm thick bone samples using a Perkin Elmer Spotlight 400 imaging spectrometer (Shelton, CT). The images were collected in the frequency range 4000–7800 cm^{-1} at 64 cm^{-1} spectral resolution and 50 μm pixel resolution with 2 co-added scans (two scans were averaged to improve signal to noise ratio). The imaging time was approximately 20 minutes for each sample. Prior to imaging, the surface sample water was dabbed dry with a Kimwipe. Care was taken to minimize water loss during imaging by keeping the sample between a glass slide and glass coverslip.

2.5 NIRSI data processing and analysis

NIR spectral images were analyzed using ISys 5.0 software (Malvern Instruments, Columbia, MD). NIR absorbances from water at ~ 5150 and ~7008 cm^{-1}, collagen at 4608 cm^{-1}, and fat (from bone marrow) at 5797 cm^{-1} were evaluated (Table 1). To process the NIRSI data, the inner trabecular regions were removed from the bone images prior to data processing by masking based on the fat absorbance (primarily from marrow) at 5797 cm^{-1}. Second derivative processing (Savitzky-Golay, 3rd order polynomial and 9 points of

smoothing) of NIR spectra was performed as a spectral resolution-enhancement technique. Although spatially resolved data were collected at 50 micron resolution, for analysis, the data were averaged across the bulk sample to compare in a manner commensurate to MRI parameters. For each sample, the integrated areas of the absorbances of interest were calculated across the entire image (N = 12). In addition, the mean second derivative peak values (inverted, to make positive) were calculated for each peak of interest, and correlated to the mean integrated areas of the peaks (N = 18). These calculations were performed to confirm that relative values from the second derivative analysis (which enable more precise peak locations to be utilized), and the integrated areas (the traditional method used to calculate relative amount of a component) were comparable. We note that although 18 tissue samples were utilized for comparison of the integrated peak areas and second derivative values, 6 of these samples could not be used for in-depth NIR spectral analysis of water, as they were left in PBS at 4° C for more than 3 days. For the 12 remaining samples, correlations between the mean NIR water peak intensities at 5152 and 7008 cm^{-1} and the MRI bound water content, the NIR-determined collagen, and the fat absorbance were also investigated. In addition, correlations were investigated between donor age and NIR-determined collagen, and water peaks at 5152 and 7008 cm^{-1}. Two data points were determined to be outliers in the 5152 cm^{-1} data set based on a Q test. Spectral data from trabecular regions were not included for correlation data. The Pearson's correlation coefficient r was reported for all correlations and significance was assessed at $p < 0.05$.

Further, evaporation studies were performed on 3 bone samples to gain insight into the environment of the water peaks, e.g., whether they arose from loosely or tightly bound water. For those samples, spectral data were collected from wet samples, and again after overnight lyophilization.

2.6 NIRSI Fat peak identification

Absorbances from water and collagen in cartilage and bone in the NIR spectral region have previously been identified by our group[62, 69, 74]. However, as the first study to evaluate NIR spectral imaging of bone with marrow, a separate experiment was performed to confirm the specific absorbances that arise from bone marrow fat. Cortical bone from bovine tibias (n=4, 2–4 month old animals) (Research 87, Boylston, MA) were cut into smaller segments of ~ 5 cm length with a bone band saw (Mar-Med Inc, Strongsville, OH) and stored in PBS at −20°C until processing. Thawed tibias were cut into 500 μm thick, cross-sectioned slices containing cortical and trabecular regions using a diamond wafering saw (Buehler Isomet). NIR spectral images of the bone slices were collected as described above. After data collection, bone marrow was removed by sonication using a Branson 2510 Ultrasonicator (Emerson Industrial Automation, Danbury, CT) with a 1% tergazyme solution for 30 minutes at 45°C. This was followed by gentle washing with water for 15 seconds. Each sample was imaged again after sonication. NIR spectral imaging data were analyzed as described above. The fat absorbance at 5797 cm^{-1} was normalized by a NIR matrix peak at 4896 cm^{-1} [66] to account for potential differences in bone thickness.

3. Results

3.1 Identification of NIR absorbances associated with specific components of bone

NIR spectra from bone were dominated by peaks at 5152 and 7008 cm^{-1}, known to arise from water absorbances [62], a peak at 4608 cm^{-1} that arises from protein (collagen [69]), a shoulder at 4896 cm^{-1} that is attributed to matrix absorbance [72, 73, 75], primarily collagen, and spectral absorbances from fat at ~5664 and 5797 cm^{-1}, which were most noticeable in trabecular bone (Figure 1a). Figure 1b shows the distribution of water in the bone based on the water absorbance at 5152 cm^{-1}. In this image each pixel results in a spectrum which contains qualitative and quantitative information about the sample. The color bar indicates the intensity of water where blue indicates low and red indicates high intensities. Figure 1c shows representative spectra from red, orange and blue regions of the figure.

There was a significant correlation between the (inverted) mean second derivative peak heights of the NIR absorbances with the mean peak integration of the water, collagen and fat NIR absorbances, respectively, indicating that either the second derivative peak heights or the raw spectra peak integration could be used to determine relative content of water or matrix components (Figure 2). The lower r value for fat is likely attributable to the broadness of the fat peak, which makes peak integration challenging. The second derivative peak for fat is much better resolved.

The distribution of collagen, water and fat content based on the second derivatives in an entire bone cross-section is shown in Figure 3. Water is present throughout the bone matrix, and also appears in the marrow region. This could arise from blood in the marrow, or from water adsorbed to fat. The images show that the 4608 cm^{-1} absorbance, which, in cartilage samples, has been shown to arise from collagen [69], does indeed appear to be specific for collagen in bone as well, as there is little to no absorbance in the marrow region. The fat peak at 5797 cm^{-1} is very specific for the marrow surrounding the trabecular bone.

The assignment of the 5797 cm^{-1} peak was further validated by ultrasonication, where the 5797 cm^{-1} absorbance completely disappeared after the sonication procedure, indicating that this absorbance is indeed a marker for fat present in the bone marrow (Figure 4).

Figure 5 shows the sensitivity of the NIR absorbances centered at ~ 5152 and 7008 cm^{-1} to water content in bone. Spectra were acquired as the bone water began to evaporate (5A, C), and for the final time point, after lyophilization (5B, D). The mean intensities of the water peak decreased two-fold for both the 5152 and 7008 cm^{-1} absorbances, respectively. In addition, shifts in the absorbances to higher frequencies were evident after lyophilization: the 5152 peak shifted to ~ 5168 $cm^{-1,}$ and the 7008 peak shifted to ~ 7040 cm^{-1}. This indicates that bound water remains, as the infrared frequency of bound water is higher than that of free water[62]. However, it is still not known whether the remaining water is bound to collagen or mineral.

3.2 Correlations of NIR spectral data and UTE data

The MRI UTE-determined bound water content in tibial cortical bone samples ranged from 62 to 91%. The NIR water peaks at 5152 cm^{-1} and at 7008 cm^{-1} correlated significantly with the UTE data, with $r = 0.735$, $p = 0.016$, and $r = 0.71$, $p = .0096$, respectively (Figure 6). There was also a strong correlation between the intensity of the NIR water peak at 7008 cm^{-1} and the intensity of the collagen peak at 4608 cm^{-1} ($r = 0.69$, $p = 0.004$). There was not a significant correlation between the NIR intensity of the water absorbance and the fat absorbance at 5797 cm^{-1} (r=0.42, p = 0.17), however, indicating that the NIR water peak is associated specifically with bone matrix. Figure 7 shows a visual comparison of the NIRS images based on 7008 cm^{-1} in bones with varying MRI-derived bound water fractions.

3.3 Correlations of donor age with NIR data

A significant inverse correlation was found between donor age and NIR-determined water using the 7008 cm^{-1} water peak ($r = -0.72$, $p = 0.009$) (Figure 8a). There was no significant correlations between donor age and water content using the 5152 cm^{-1} peak, or between donor age and collagen based on the 4608 cm^{-1} peak. However, a dual-parameter linear regression model based on donor age and intensity of the collagen peak at 4608 cm^{-1} was able to account for 65% of the variance ($p = 0.0093$) present in the MRI bound water fraction (Figure 8b).

4.0 Discussion

Here, we describe for the first time the application of near infrared spectral imaging (NIRSI) for evaluation of water and the organic components of bone, studied at microscopic spatial resolution, in a cross-section of human bone. Two primary absorbances from water, an absorbance from collagen, and absorbances from fat (primarily in bone marrow) were identified and used to view the distribution of these components in sections of tibial bone. The bone samples investigated came from a range of ages, and showed a range of compositional parameters. Although the data were reported as averages across samples, spatial resolution of water and collagen can also be investigated in whole tissue segments. For example, it could be interesting to evaluate compositional parameters in fracture healing or in different disease models of bone, such as osteogenesis imperfecta (OIM) or osteoporotic mice [31, 76].

NIRSI data associated with the inorganic mineral component of bone, typically carbonate-substituted hydroxyapatite, were not directly investigated here. Although mid-infrared spectral analysis is frequently utilized to evaluate mineral quality in bone, including in imaging mode [17, 41, 77], the NIR spectral region is not ideal for this type of evaluations. Mid-infrared spectral absorbances from apatite and other calcium phosphates arise primarily from the phosphate component, and the contour and frequencies of the phosphate absorbances are spectral fingerprints for the type and amount of mineral present in tissue [34]. In contrast, there is no phosphate (PO_4) absorbance in the NIR spectral region[64]. However, there are small absorbances from P-OH moities of hydroxyapatite, and from water on the surface or bound to the mineral phase[64]. Understanding these absorbances could

indeed be helpful for investigation of bone quality, but the challenge of confirming these low-intensity absorbances in intact bone requires a separate thorough investigation.

Researchers conducting preclinical studies have investigated multiple parameters associated with bone quality, primarily mineral content and bone architecture [17, 21] and, more recently, the collagen content and crosslinks [39]. To a much lesser extent, water content was also studied. It is clear that a limiting factor in the investigation of water in bone is the lack of an appropriate laboratory tool for such studies. Although gravimetric analyses can be performed [50, 52], such studies leave the tissues of interest dehydrated, and not suitable for most further analyses. We envision NIRSI being useful for assessment of water content at high spatial resolution in animal models of disease and for evaluation of the effect of therapeutics on bone quality. In this study, our aim was twofold, to establish the feasibility of NIRS to study water and matrix content in intact bone samples, and to compare the outcomes of our methods with bulk measurements from MRI water content (a gold standard for water content evaluation); therefore, we restricted ourselves to reporting the bulk outcomes rather than the spatial information. That being said, the ability to collect data at microscopic resolution could be used to study the distribution of water associated with mineral and collagen at the pore and microstructural level. The NIRS technique developed in this manuscript allows us to collect spectral data from the bone samples at ~6 μm spatial resolution. In these NIRS images, each pixel results in a spectrum which contains qualitative and quantitative information about the sample.

Given the penetration depth of the NIR radiation, which is on the order of millimeters in the spectral regions of interest [78], it is likely that intact pieces of mouse bone can be sampled by NIRSI for water evaluation. Further, interrogation of bone can also be performed using NIR fiber optics [74], although at a spatial resolution on the order of ~ 1 mm. Nevertheless, NIR fiber optics and the spectrometers they are coupled to are generally reasonably priced, similar to many other standard types of lab equipment.

MRI UTE studies of bone water are increasing, as are correlations of these data to bone's mechanical parameters [4, 43, 44, 46], which could reflect a measure of fracture risk. Here, we demonstrated correlations of NIRSI data to UTE data, suggesting that both techniques are sensitive to water bound to the collagen component of bone [47, 48]. With the NIR modality, we can now also investigate whether changes in collagen, such as those that occur in genetic bone diseases [31, 79], or in osteoporosis [80], and with potential therapeutic interventions[10, 81, 82], affect the optimal water content of bone. In addition, the demonstration of correlation of donor age to the NIR-determined water content supports further investigations into the utility of the NIR technique. It has previously been shown that UTE-determined collagen-bound water is inversely correlated to age [45]; here, we confirm that NIR-determined data on water content mirrors those findings.

Interestingly, even though both the 7008 and 5152 cm^{-1} water absorbances both correlated directly to the UTE bound water data, only the 7008 cm^{-1} water absorbance was inversely correlated with donor age. This indicates that origins of these water absorbances, and the environments they are in, are likely not identical. Possible environments for these water absorbances are pore water, loosely bound to mineral or collagen, structurally incorporated

into mineral or collagen, or a combination of these. Further, there could also be contributions from non-water OH bonds, such as from P-OH on the surface or within the apatite crystals[64]. There are several water compartments in collagen, including surface, within the triple helical structure, or connecting helices that are within the same fibril [83]. Clearly, further detailed studies, which will include deuterium exchange to enable the identification of specific water compartments [42, 48, 84], will be required to better understand the nature of these absorbances.

Even with the current limited understanding of which specific tissue entity water is bound to, NIR spectral imaging data can yield insight into the distribution of water at micron spatial resolution, which is a very useful tool for evaluation of a parameter that contributes to bone quality. Further, the water distribution can also be evaluated in the context of mineral and collagen parameters determined by mid-infrared imaging evaluation on the same sample at similar resolution using attenuated total reflectance imaging [85, 86]. Together, we can obtain information on how perturbations in collagen structure, such as crosslink abnormalities, genetic diseases, or therapeutic interventions, affect bone quality based on disruptions in the mineralization process and/or in water binding, and, ultimately, how this leads to bone quality deficits.

5.0 Conclusion

In this study, for the first time, NIR spectral imaging was used for the evaluation of the spatial distribution of water and organic components of a cross-section of human bone. Our results showed that NIRSI parameters significantly correlated with MRI UTE data, suggesting that NIR could be a very useful tool to study parameters affecting bone quality. Further studies are required for the assignment of NIR water absorbances related to the mineral phase and content.

Acknowledgments

This study was supported by NIH R01 AR056145 and NIH R21 AR071704.

References

1. Bala Y, Zebaze R, Ghasem-Zadeh A, Atkinson EJ, Iuliano S, Peterson JM, Amin S, Bjornerem A, Melton LJ 3rd, Johansson H, Kanis JA, Khosla S, Seeman E. Cortical porosity identifies women with osteopenia at increased risk for forearm fractures. J Bone Miner Res. 2014; 29(6):1356–62. [PubMed: 24519558]
2. Evans FG. Mechanical properties and histology of cortical bone from younger and older men. Anat Rec. 1976; 185(1):1–11. [PubMed: 1267192]
3. Nyman JS, Makowski AJ. The Contribution of the Extracellular Matrix to the Fracture Resistance of Bone. Current Osteoporosis Reports. 2012; 10(2):169–177. [PubMed: 22527725]
4. Rajapakse CS, Leonard MB, Bhagat YA, Sun W, Magland JF, Wehrli FW. Micro-MR imaging-based computational biomechanics demonstrates reduction in cortical and trabecular bone strength after renal transplantation. Radiology. 2012; 262(3):912–20. [PubMed: 22357891]
5. Zioupos P, Currey JD. Changes in the stiffness, strength, and toughness of human cortical bone with age. Bone. 1998; 22(1):57–66. [PubMed: 9437514]
6. Farr JN, Drake MT, Amin S, Melton LJ 3rd, McCready LK, Khosla S. In vivo assessment of bone quality in postmenopausal women with type 2 diabetes. J Bone Miner Res. 2013; 29(4):787–95.

7. Nyandege AN, Slattum PW, Harpe SE. Risk of Fracture and the Concomitant Use of Bisphosphonates With Osteoporosis-Inducing Medications. Ann Pharmacother. 2015
8. Ahmad F, Yunus SM, Asghar A, Faruqi NA. Influence of anabolic steroid on tibial fracture healing in rabbits - a study on experimental model. J Clin Diagn Res. 2013; 7(1):93–6. [PubMed: 23449755]
9. Mashiba T, Turner CH, Hirano T, Forwood MR, Johnston CC, Burr DB. Effects of suppressed bone turnover by bisphosphonates on microdamage accumulation and biomechanical properties in clinically relevant skeletal sites in beagles. Bone. 2001; 28(5):524–31. [PubMed: 11344052]
10. Boskey AL. Bone composition: relationship to bone fragility and antiosteoporotic drug effects. Bonekey Rep. 2014; 2:447.
11. Nickolas TL, Stein E, Cohen A, Thomas V, Staron RB, McMahon DJ, Leonard MB, Shane E. Bone mass and microarchitecture in CKD patients with fracture. J Am Soc Nephrol. 2010; 21(8): 1371–80. [PubMed: 20395370]
12. Ito M, Wakao N, Hida T, Matsui Y, Abe Y, Aoyagi K, Uetani M, Harada A. Analysis of hip geometry by clinical CT for the assessment of hip fracture risk in elderly Japanese women. Bone. 2010; 46(2):453–7. [PubMed: 19735752]
13. Ito M, Nakamura T, Matsumoto T, Tsurusaki K, Hayashi K. Analysis of trabecular microarchitecture of human iliac bone using microcomputed tomography in patients with hip arthrosis with or without vertebral fracture. Bone. 1998; 23(2):163–9. [PubMed: 9701476]
14. Zioupos P. Ageing human bone: factors affecting its biomechanical properties and the role of collagen. J Biomater Appl. 2001; 15(3):187–229. [PubMed: 11261600]
15. Zioupos P, Currey JD, Hamer AJ. The role of collagen in the declining mechanical properties of aging human cortical bone. J Biomed Mater Res. 1999; 45(2):108–16. [PubMed: 10397964]
16. Wang X, Bank RA, TeKoppele JM, Agrawal CM. The role of collagen in determining bone mechanical properties. J Orthop Res. 2001; 19(6):1021–6. [PubMed: 11781000]
17. Gourion-Arsiquaud S, Lukashova L, Power J, Loveridge N, Reeve J, Boskey AL. Fourier transform infrared imaging of femoral neck bone: reduced heterogeneity of mineral-to-matrix and carbonate-to-phosphate and more variable crystallinity in treatment-naive fracture cases compared with fracture-free controls. J Bone Miner Res. 2013; 28(1):150–61. [PubMed: 22865771]
18. Nyman JS, Gorochow LE, Adam Horch R, Uppuganti S, Zein-Sabatto A, Manhard MK, Does MD. Partial removal of pore and loosely bound water by low-energy drying decreases cortical bone toughness in young and old donors. J Mech Behav Biomed Mater. 2013; 22:136–45. [PubMed: 23631897]
19. Samuel J, Sinha D, Zhao JC, Wang X. Water residing in small ultrastructural spaces plays a critical role in the mechanical behavior of bone. Bone. 2013; 59:199–206. [PubMed: 24291421]
20. Yan J, Daga A, Kumar R, Mecholsky JJ. Fracture toughness and work of fracture of hydrated, dehydrated, and ashed bovine bone. J Biomech. 2008; 41(9):1929–36. [PubMed: 18502430]
21. Hui SL, Slemenda CW, Johnston CC Jr. Age and bone mass as predictors of fracture in a prospective study. J Clin Invest. 1988; 81(6):1804–9. [PubMed: 3384952]
22. Kanis JA, Johnell O, Oden A, Dawson A, De Laet C, Jonsson B. Ten year probabilities of osteoporotic fractures according to BMD and diagnostic thresholds. Osteoporos Int. 2001; 12(12): 989–95. [PubMed: 11846333]
23. Techawiboonwong A, Song HK, Leonard MB, Wehrli FW. Cortical bone water: in vivo quantification with ultrashort echo-time MR imaging. Radiology. 2008; 248(3):824–33. [PubMed: 18632530]
24. Genant HK, Boyd D. Quantitative bone mineral analysis using dual energy computed tomography. Invest Radiol. 1977; 12(6):545–51. [PubMed: 591258]
25. Link TM. Osteoporosis imaging: state of the art and advanced imaging. Radiology. 2012; 263(1): 3–17. [PubMed: 22438439]
26. Zebaze R, Ghasem-Zadeh A, Mbala A, Seeman E. A new method of segmentation of compact-appearing, transitional and trabecular compartments and quantification of cortical porosity from high resolution peripheral quantitative computed tomographic images. Bone. 2013; 54(1):8–20. [PubMed: 23334082]

27. Chang G, Honig S, Brown R, Deniz CM, Egol KA, Babb JS, Regatte RR, Rajapakse CS. Finite element analysis applied to 3-T MR imaging of proximal femur microarchitecture: lower bone strength in patients with fragility fractures compared with control subjects. Radiology. 2014; 272(2):464–74. [PubMed: 24689884]
28. Patsch JM, Burghardt AJ, Kazakia G, Majumdar S. Noninvasive imaging of bone microarchitecture. Ann N Y Acad Sci. 2011; 1240:77–87. [PubMed: 22172043]
29. Pleshko N, Boskey A, Mendelsohn R. Novel Infrared Spectroscopic Method for the Determination of Crystallinity of Hydroxyapatite Mineral. Biophysical Journal. 1991; 60(4):786–793. [PubMed: 1660314]
30. Camacho NP, Raggio CL, Doty SB, Root L, Zraick V, Ilg WA, Toledano TR, Boskey AL. A controlled study of the effects of alendronate in a growing mouse model of osteogenesis imperfecta. Calcified Tissue International. 2001; 69(2):94–101. [PubMed: 11683430]
31. Camacho NP, Landis WJ, Boskey AL. Mineral changes in a mouse model of osteogenesis imperfecta detected by Fourier transform infrared microscopy. Connective Tissue Research. 1996; 35(1–4):259–265. [PubMed: 9084664]
32. Camacho NP, Hou L, Toledano TR, Ilg WA, Brayton CF, Raggio CL, Root L, Boskey AL. The material basis for reduced mechanical properties in oim mice bones. Journal of Bone and Mineral Research. 1999; 14(2):264–272. [PubMed: 9933481]
33. Boskey AL, Pleshko N, Doty SB, Mendelsohn R. Applications of fourier-transform infrared (ft-ir) microscopy to the study of mineralization in bone and cartilage. Cells and Materials. 1992; 2(3): 209–220.
34. Boskey A, Camacho NP. FT-IR imaging of native and tissue-engineered bone and cartilage. Biomaterials. 2007; 28(15):2465–2478. [PubMed: 17175021]
35. Camacho NP, Carroll P, Raggio CL. Fourier transform infrared imaging spectroscopy (FT-IRIS) of mineralization in bisphosphonate-treated oim/oim mice. Calcified Tissue International. 2003; 72(5):604–609. [PubMed: 12574874]
36. Raghavan M, Sahar ND, Wilson RH, Mycek MA, Pleshko N, Kohn DH, Morris MD. Quantitative polarized Raman spectroscopy in highly turbid bone tissue. Journal of Biomedical Optics. 2010; 15(3)
37. Mandair GS, Morris MD. Contributions of Raman spectroscopy to the understanding of bone strength. Bonekey Rep. 2015; 4:620. [PubMed: 25628882]
38. Morris MD, Finney WF. Recent developments in Raman and infrared spectroscopy and imaging of bone tissue. Spectroscopy. 2004; 18:155–159.
39. Saito M, Marumo K. Collagen cross-links as a determinant of bone quality: a possible explanation for bone fragility in aging, osteoporosis, and diabetes mellitus. Osteoporos Int. 2010; 21(2):195–214. [PubMed: 19760059]
40. Nyman JS, Roy A, Acuna RL, Gayle HJ, Reyes MJ, Tyler JH, Dean DD, Wang X. Age-related effect on the concentration of collagen crosslinks in human osteonal and interstitial bone tissue. Bone. 2006; 39(6):1210–7. [PubMed: 16962838]
41. Gourion-Arsiquaud S, Faibish D, Myers E, Spevak L, Compston J, Hodsman A, Shane E, Recker RR, Boskey ER, Boskey AL. Use of FTIR spectroscopic imaging to identify parameters associated with fragility fracture. J Bone Miner Res. 2009; 24(9):1565–71. [PubMed: 19419303]
42. Unal M, Yang S, Akkus O. Molecular spectroscopic identification of the water compartments in bone. Bone. 2014; 67:228–36. [PubMed: 25065717]
43. Bae WC, Chen PC, Chung CB, Masuda K, D'Lima D, Du J. Quantitative ultrashort echo time (UTE) MRI of human cortical bone: correlation with porosity and biomechanical properties. J Bone Miner Res. 2011; 27(4):848–57.
44. Horch RA, Gochberg DF, Nyman JS, Does MD. Non-invasive predictors of human cortical bone mechanical properties: T(2)-discriminated H NMR compared with high resolution X-ray. PLoS One. 2011; 6(1):e16359. [PubMed: 21283693]
45. Rajapakse CS, Bashoor-Zadeh M, Li C, Sun W, Wright AC, Wehrli FW. Volumetric cortical bone porosity assessment with MR imaging: validation and clinical feasibility. Radiology. 2015; 276(2): 526–535. [PubMed: 26203710]

46. Bae WC, Ruangchaijatuporn T, Chang EY, Biswas R, Du J, Statum S, Chung CB. MR morphology of triangular fibrocartilage complex: correlation with quantitative MR and biomechanical properties. Skeletal Radiol. 2016; 45(4):447–54. [PubMed: 26691643]
47. Manhard MK, Horch RA, Harkins KD, Gochberg DF, Nyman JS, Does MD. Validation of Quantitative Bound- and Pore-Water Imaging in Cortical Bone. Magnetic Resonance in Medicine. 2014; 71(6):2166–2171. [PubMed: 23878027]
48. Ong HH, Wright AC, Wehrli FW. Deuterium Nuclear Magnetic Resonance Unambiguously Quantifies Pore and Collagen-Bound Water in Cortical Bone. Journal of Bone and Mineral Research. 2012; 27(12):2573–2581. [PubMed: 22807107]
49. Seifert AC, Li C, Rajapakse CS, Bashoor-Zadeh M, Bhagat YA, Wright AC, Zemel BS, Zavaliangos A, Wehrli FW. Bone mineral (31)P and matrix-bound water densities measured by solid-state (31)P and (1)H MRI. NMR Biomed. 2014; 27(7):739–48. [PubMed: 24846186]
50. Allen MR, Territo PR, Lin C, Persohn S, Jiang L, Riley AA, McCarthy BP, Newman CL, Burr DB, Hutchins GD. In vivo UTE-MRI Reveals Positive Effects of Raloxifene on Skeletal Bound Water in Skeletally Mature Beagle Dogs. J Bone Miner Res. 2015
51. Du J, Bydder GM. Qualitative and quantitative ultrashort-TE MRI of cortical bone. NMR Biomed. 2013; 26(5):489–506. [PubMed: 23280581]
52. Unal M, Akkus O. Raman spectral classification of mineral- and collagen-bound water's associations to elastic and post-yield mechanical properties of cortical bone. Bone. 2015; 81:315–26. [PubMed: 26211992]
53. Büning-Pfaue H. Analysis of water in food by near infrared spectroscopy. Food Chemistry. 2003; 82(1):9.
54. Jamrogiewicz M. Application of the near-infrared spectroscopy in the pharmaceutical technology. J Pharm Biomed Anal. 2012; 66:1–10. [PubMed: 22469433]
55. dos Santos CA, Lopo M, Pascoa RN, Lopes JA. A review on the applications of portable near-infrared spectrometers in the agro-food industry. Appl Spectrosc. 2013; 67(11):1215–33. [PubMed: 24160873]
56. Zhou GX, Ge Z, Dorwart J, Izzo B, Kukura J, Bicker G, Wyvratt J. Determination and differentiation of surface and bound water in drug substances by near infrared spectroscopy. J Pharm Sci. 2003; 92(5):1058–65. [PubMed: 12712426]
57. Luypaert J, Massart DL, Vander Heyden Y. Near-infrared spectroscopy applications in pharmaceutical analysis. Talanta. 2007; 72(3):865–83. [PubMed: 19071701]
58. Bock JE, Connelly RK. Innovative uses of near-infrared spectroscopy in food processing. J Food Sci. 2008; 73(7):R91–8. [PubMed: 18803725]
59. Bowker B, Hawkins S, Zhuang H. Measurement of water-holding capacity in raw and freeze-dried broiler breast meat with visible and near-infrared spectroscopy. Poult Sci. 2014; 93(7):1834–41. [PubMed: 24864280]
60. Givens DI, De Boever JL, Deaville ER. The principles, practices and some future applications of near infrared spectroscopy for predicting the nutritive value of foods for animals and humans. Nutr Res Rev. 1997; 10(1):83–114. [PubMed: 19094259]
61. Wu D, Sun D-W. Application of visible and near infrared hyperspectral imaging for non-invasively measuring distribution of water-holding capacity in salmon flesh. Talanta. 2013; 116:266–276. [PubMed: 24148403]
62. Padalkar MV, Spencer RG, Pleshko N. Near Infrared Spectroscopic Evaluation of Water in Hyaline Cartilage. Ann Biomed Eng. 2013; 41(11):1–11. [PubMed: 23053297]
63. Lammertyn J, Peirs A, De Baerdemaeker J, Nicolaı B. Light penetration properties of NIR radiation in fruit with respect to non-destructive quality assessment. Postharvest Biology and Technology. 2000; 18(2):121–132.
64. Kolmas J, Marek D, Kolodziejski W. Near-Infrared (NIR) Spectroscopy of Synthetic Hydroxyapatites and Human Dental Tissues. Applied spectroscopy. 2015; 69(8):902–912. [PubMed: 26163232]
65. Blanco M, Villarroya I. NIR spectroscopy: a rapid-response analytical tool. TrAC Trends in Analytical Chemistry. 2002; 21(4):240–250.
66. Larkin, P. Infrared and Raman spectroscopy: principles and spectral interpretation. Elsevier; 2011.

67. Timlin JA, Carden A, Morris MD, Bonadio JF, Hoffler CE, Kozloff KM, Goldstein SA. Spatial distribution of phosphate species in mature and newly generated mammalian bone by hyperspectral Raman imaging. Journal of Biomedical Optics. 1999; 4(1):28–34. [PubMed: 23015166]
68. Chalmers, JM., Edwards, HG., Hargreaves, MD. Infrared and Raman spectroscopy in forensic science. John Wiley & Sons; 2012.
69. Palukuru UP, McGoverin CM, Pleshko N. Assessment of hyaline cartilage matrix composition using near infrared spectroscopy. Matrix Biology. 2014; 38:3–11. [PubMed: 25083813]
70. Rajapakse CS, Bashoor-Zadeh M, Li C, Sun W, Wright AC, Wehrli FW. Volumetric Cortical Bone Porosity Assessment with MR Imaging: Validation and Clinical Feasibility. Radiology. 2015:141850.
71. Luck, WAP. Structure of water and aqueous solutions. In: Luck, WAP., editor. Proceedings of the International Symposium held at Marburg; July 1973; Marburg. 1974.
72. Liu Y, Cho R-K, Sakuri K, Miura T, Ozaki Y. Studies on spectra/structure correlations in near-infrared spectra of proteins and polypeptides. Part I: A marker band for hydrogen bonds. Applied spectroscopy. 1994; 48(10):1249–1254.
73. Šašić S, Ozaki Y. Band assignment of near-infrared spectra of milk by use of partial least-squares regression. Applied spectroscopy. 2000; 54(9):1327–1338.
74. McGoverin CM, Lewis K, Yang X, Bostrom MPG, Pleshko N. The Contribution of Bone and Cartilage to the Near-Infrared Spectrum of Osteochondral Tissue. Applied Spectroscopy. 2014; 68(10):1168–1175. [PubMed: 25197817]
75. Liu Y, Cho R-K, Sakurai K, Miura T, Ozaki Y. Studies on spectra/structure correlations in near-infrared spectra of proteins and polypeptides. Part I: A marker band for hydrogen bonds. Applied spectroscopy. 1994; 48(10):1249–1254.
76. Boskey AL. Bone composition: relationship to bone fragility and antiosteoporotic drug effects. BoneKEy reports. 2013; 2
77. Grabner BM, Camacho N, Roschger P, Zizak I, Klaushofer K, Fratzl P. Effect of alendronate on bone mineralization density in the osteogenesis imperfecta murine model and wild type controls. Journal of Bone and Mineral Research. 2000; 15:S338–S338.
78. Padalkar MV, Pleshko N. Wavelength-dependent penetration depth of near infrared radiation into cartilage. Analyst. 2015
79. Bargman R, Posham R, Boskey AL, DiCarlo E, Raggio C, Pleshko N. Comparable outcomes in fracture reduction and bone properties with RANKL inhibition and alendronate treatment in a mouse model of osteogenesis imperfecta. Osteoporosis International. 2012; 23(3):1141–1150. [PubMed: 21901481]
80. Bailey A, Wotton S, Sims T, Thompson P. Biochemical changes in the collagen of human osteoporotic bone matrix. Connective tissue research. 1993; 29(2):119–132. [PubMed: 8403893]
81. Garnero P. The role of collagen organization on the properties of bone. Calcified tissue international. 2015; 97(3):229–240. [PubMed: 25894071]
82. Nyman JS, Ni QW, Nicolella DP, Wang XD. Measurements of mobile and bound water by nuclear magnetic resonance correlate with mechanical properties of bone. Bone. 2008; 42(1):193–199. [PubMed: 17964874]
83. Bella J, Eaton M, Brodsky B, Berman HM. Crystal and molecular structure of a collagen-like peptide at 1.9 A resolution. Science. 1994; 266(5182):75–81. [PubMed: 7695699]
84. Gul-E-Noor F, Singh C, Papaioannou A, Sinha N, Boutis GS. Behavior of Water in Collagen and Hydroxyapatite Sites of Cortical Bone: Fracture, Mechanical Wear, and Load Bearing Studies. The Journal of Physical Chemistry C. 2015; 119(37):21528–21537.
85. Gulley-Stahl HJ, Bledsoe SB, Evan AP, Sommer AJ. The advantages of an attenuated total internal reflection infrared microspectroscopic imaging approach for kidney biopsy analysis. Applied spectroscopy. 2010; 64(1):15–22. [PubMed: 20132593]
86. Kazarian SG, Chan KL, Maquet V, Boccaccini AR. Characterisation of bioactive and resorbable polylactide/Bioglass composites by FTIR spectroscopic imaging. Biomaterials. 2004; 25(18): 3931–8. [PubMed: 15046883]

Highlights

- Structural water has been identified as an important contributor to bone quality.
- There are no standard modalities to evaluate the distribution of water at the microscopic level.
- We demonstrated that near infrared spectroscopic imaging (NIRSI) can assess the distribution of collagen, fat and water in bone at microscopic resolution.
- NIRSI analysis of water correlated significantly with MRI UTE-determined percentage of water in human bone.

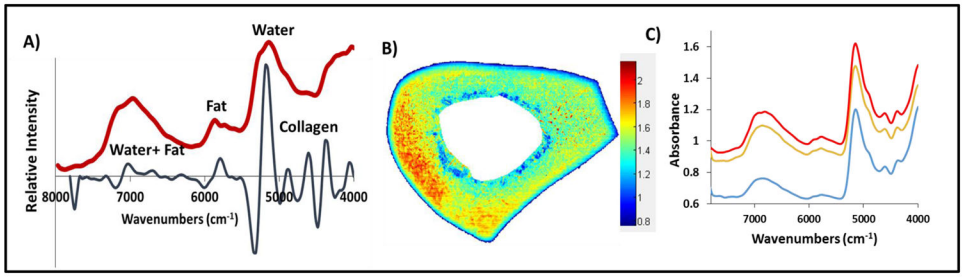

Figure 1.

A) Raw NIR imaging spectrum (red) obtained from a region of trabecular bone; Second derivative spectrum (black) shows the resolution enhancement of absorbances. B) NIR spectral image based on water absorbance at 5152 cm^{-1} C) Stacked NIR spectra from bone where color of the spectrum represents the region they were obtained from in image B.

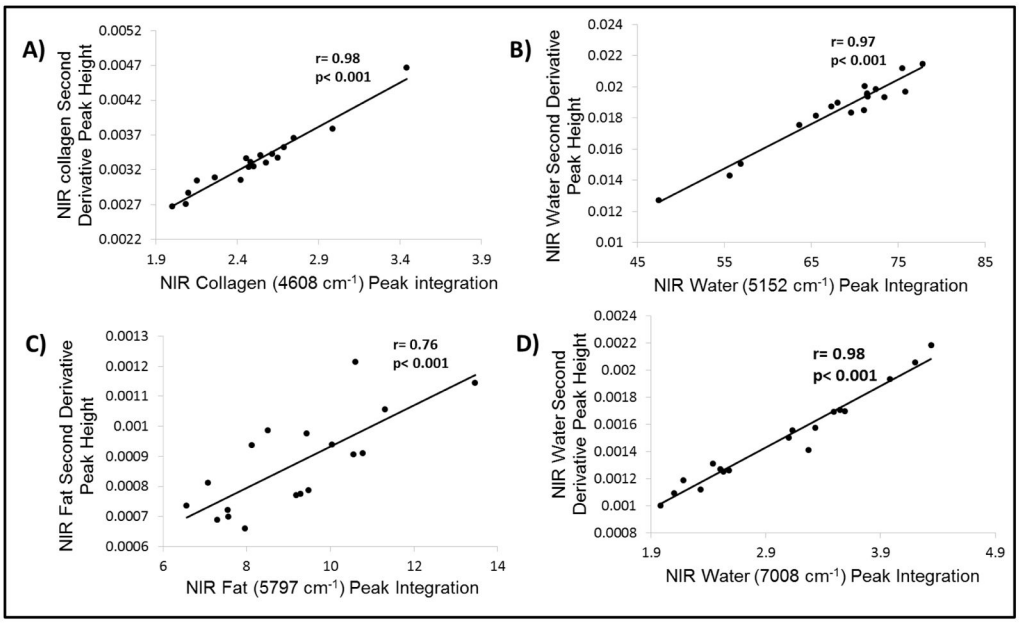

Figure 2.

Correlation graphs and coefficients between the inverted second derivative peak heights and peak integration areas obtained from NIRS images of bone samples.

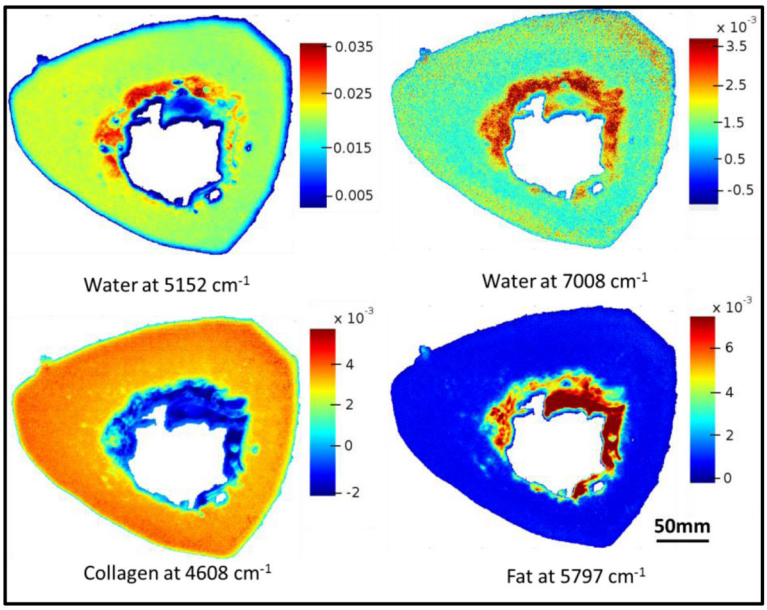

Figure 3.

NIR spectral images based on second derivatives, showing water distribution (5152 cm^{-1} and 7008 cm^{-1}), collagen (4608 cm^{-1}) and fat (5797 cm^{-1}) in an entire bone cross-section. Scale bars reflect inverted second derivative peak height intensities, where red is highest and blue is lowest.

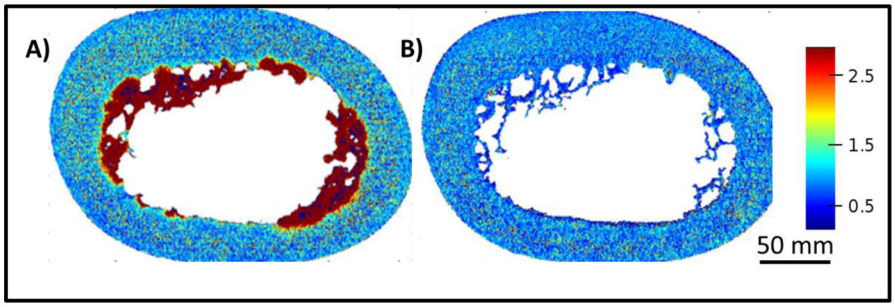

Figure 4.

NIR spectral images of bovine bone before (A) and after (B) sonication for 30 minutes. The images were generated by normalizing the NIR fat absorbance at 5797 cm^{-1} to the matrix peak at 4896 cm^{-1}. The scale bar reflects peak height ratio.

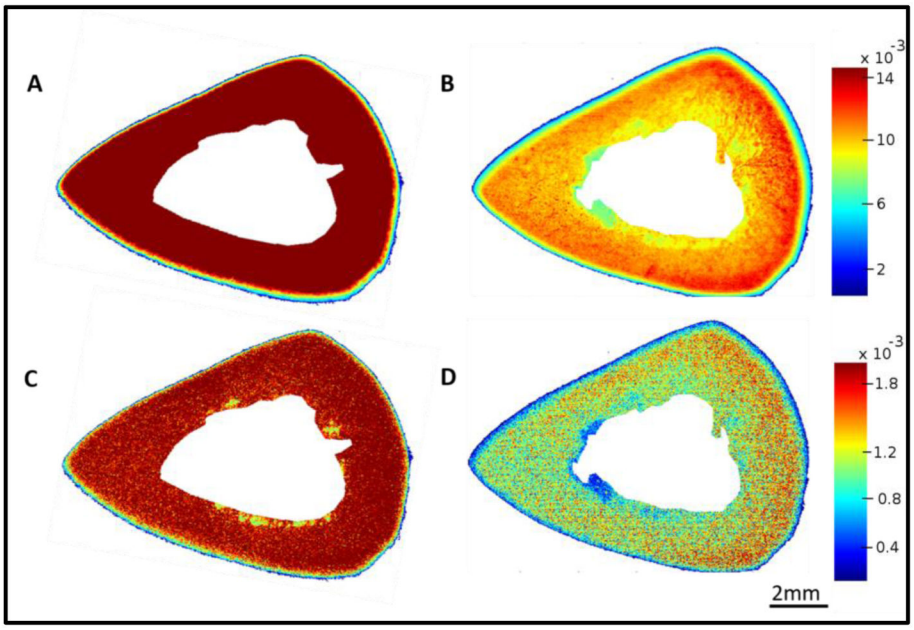

Figure 5.

NIR spectral images of a bone section sampled at 50 μm pixel resolution based on distribution of water absorbances at 5152 (A) and 7008 (C) cm^{-1} before lyophilyzation, and after lyophilyzation (5152 (B),7008 (D)). Scale bars reflect inverted second derivative peak height intensities.

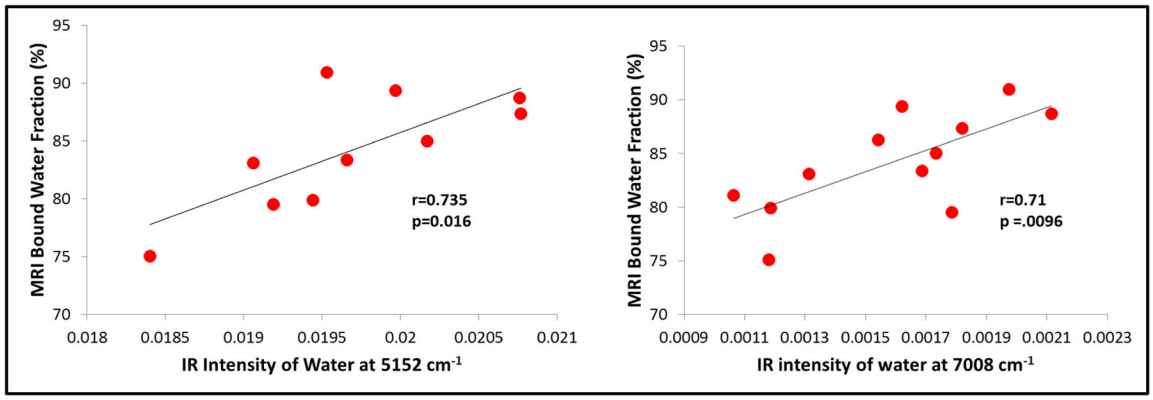

Figure 6.

Correlation of MRI-derived bound water fraction and NIRSI-derived intensities from water at 5152 cm^{-1} and 7008 cm^{-1}.

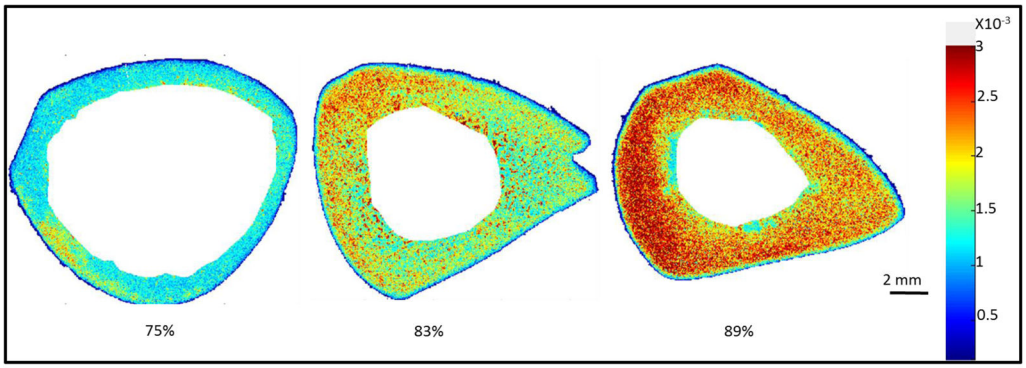

Figure 7.

A visual comparison of NIRS images of bone based on the absorbance at 7008 cm^{-1} with varying MRI-derived bound water fraction (percentages below each image).

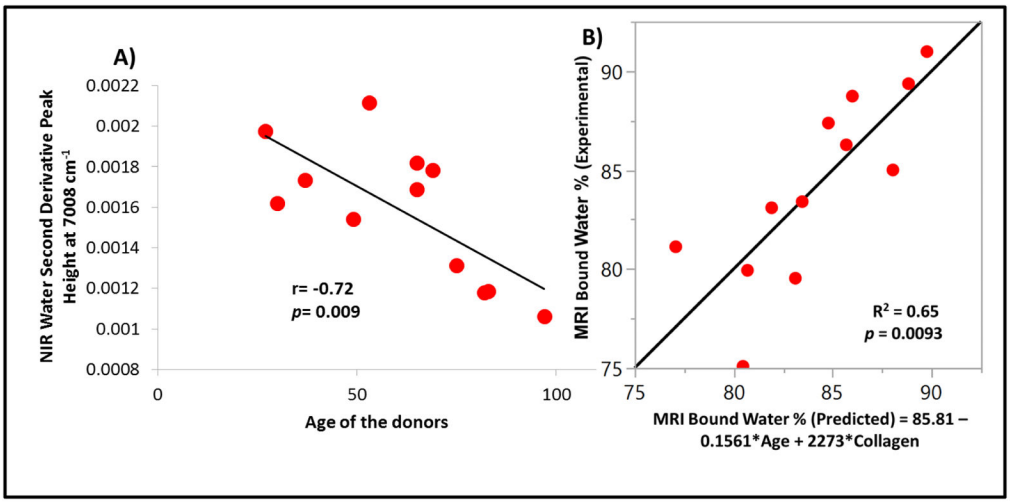

Figure 8.

Correlation between NIR-derived water content and age of the donor (A), and Predictability of MRI-derived bound water fraction using donor age and NIR-derived collagen measurements (B).

Table 1

NIR absorbance band assignments for major components of bone

Component	NIR Frequency (cm^{-1})	Assignment
Water	5100 – 5200	Combination of the O-H stretching band and the O-H bending band [71]
	6900 – 7100	O-H stretching band 1st overtone [71]
Collagen	4608	Combination of the C-H stretching and the C-H deformation[69]
	4896	Combination of Amide A and II [72]
Fat	4273	Combination of CH2 symmetric stretching and bending vibrations [73]
	4344	Combination of CH2 asymmetric stretching and bending vibrations [73]
	5664–5701	1st overtone of CH2 symmetric stretching[73]
	5797	1st overtone of CH2 antisymmetric stretching [73]
Mineral (very small absorbance)	4690, 4673, 4657, 4615, 5200	Surface P-OH: combination of bending and stretching[64]
	7186, 7164, 7145, 7115	Surface P–OH: 2nd overtone (counterparts of the 4690–4615 cm-$^{-1}$ bands) [64]